Four-quadrant Force Control with Minimal Ripple for Linear Switched Reluctance Machines

Xuanrui Huang, *Member, IEEE*, Zechuan Lin, and Xi Xiao, *Member, IEEE*

Abstract: Linear switch reluctance machine (LSRM) has been tried to act as an alternative generator for direct drive linear wave energy converter (WEC). Many researchers have proposed new topologies of LSRM to improve the power density, efficiency and reliability. However, the control methods for LSRM applied in direct drive WEC have been paid little attention, especially control methods considering the wave energy generator operating characteristics. In this paper, according to the generator control requirements of the direct drive WEC, force control algorithm for LSRM operating in four quadrants without a speed closed loop is put forward. The force ripple of LSRM is suppressed using force sharing function method. The four-quadrant control is easy to realize requiring only phase currents information. Simulation results validate the proposed method and indicate that LSRM is able to be used as the generator for direct drive WEC.

***Index Terms*-Linear switched reluctance machine, direct drive wave energy converter, force ripple suppression, four-quadrant operation.**

I. INTRODUCTION

WAVE energy is a promising green and renewable energy. Direct drive WEC employs a structure that a linear generator directly connected to a float driven by the ocean waves. This kind of structure minimizes the energy loss from waves to generator and shows better efficiency. Unlike conventional generators rotating at a high and constant speed unidirectional in thermal or hydro power plants, the WEC generator is reciprocating vertically at a low speed with varying external forces in force mode without speed closed-loop. Besides, the generator will have to operate as a motor in part of time to maximize the wave energy conversion [1]. That is to say, a WEC generator is operating in four-quadrant force mode with accurate force control. This brings challenges for WEC generator design and control.

Linear permanent magnet synchronous machine (LPMSM), which has the best control performance and power density, is the first choice as the generator of the direct drive WEC. However, high costs of permanent magnets and the maintenance costs under the harsh marine environment bring some difficulties. The magnets in LPMSM will be easily demagnetized in case of vibration, high temperature and moist, being a risk [2]. Therefore, some alternative generators with none magnets are proposed for direct drive WEC, including linear induction machines (LIM) and linear switched reluctance machines (LSRM).

LSRMs have been proven to be an attractive candidate for linear direct drive applications with low cost, high reliability and fault tolerance capability [3]. Besides, LSRM can generate more force than LIM with less thermal problems [4]. Therefore, LSRMs are considered as an alternative machine for DDLWEC [5]. In [6], a tubular LSRM is presented with flexible performance and high reliability, however, it is subject to low power density and efficiency. Reference [7] presents a high power density tubular LSRM which consists of series of ferrite magnetic rings instead of the laminated salient teeth to realize better utilization of material and lower cost.

Accurate force control is one of the control requirements of WEC generator. However, the major drawback of LSRM is the force ripple due to its nonlinear inductance characteristics and the turn on and off control. The significant force ripple during phase commutation results in noise, vibration, and perhaps conversion efficiency decreases in WEC. Typical force ripple suppression methods are direct force control and force sharing function (FSF) method. Based on the relations between instantaneous force and different switch states of the drive circuit, the former method controls the switch states to suppress force ripple according to the difference between force reference and actual force [8]. Force sensors or observers are required to realize direct force control, which reduces the utility. Besides, hysteresis current controller used in direct force control will lead to relatively large current ripple, which will increase force ripple. Since the force ripple in LSRM comes from the mismatch of the phase forces during commutation, FSF suppresses the ripple by assigning force reference to each phase to keep the total force stable, and then the current reference of each phase can be calculated based on LSRM characteristics and controlled through PWM algorithm. The force sharing function is defined as the function of phase force reference to the mover position of LSRM. In classic FSF, a specific function is selected. Taking a linear function as an example, the force reference is linearly changing with the mover position during commutation. In addition, cubic, sinusoidal and exponential functions are also used as the FSF [9]. FSF with specific functions is easy to realize, while loss and current change rate limit are not considered. Another

Manuscript was submitted for review on 22, January, 2020.

This work was supported in part by the National Natural Science Foundation of China under Grant U1806224, 61733010 and in part by the Guangdong Key Research and Development Program under Grant 2019B090917001. (*Corresponding Author*: Xi Xiao)

X. Huang, Z. Lin and X. Xiao are with Department of Electrical Engineering, Tsinghua University, Beijing 100084, China. (email: hxr503@gmail.com;zechuanlin@126.com;xiao_xi@mail.tsinghua.edu.cn)

Digital Object Identifier 10.30941/CESTEMS.2020.00005

approach is to use optimization techniques to calculate the current reference. The core idea is optimizing the objective function on the premise that the total force equals the reference. In [10], the p-norm of the phase current is minimized. In addition to phase current, its rate of change and motor flux can be optimized [11].In FSF, the incoming and outgoing phase current references may change rapidly and therefore novel drive circuit topologies and current control methods are also crucial [12]. In addition to ripple suppression by control strategies, the force ripple can be also mitigated through geometric structure modification [13].

Unlike the permanent magnet machines that can be easily controlled in four quadrants, the four-quadrant operation for the LSRM is kind of complicated. The control strategies in different quadrants are not the same. In general, the core idea of four-quadrant operation for SRM is to switch control strategy based on working condition [14]. The most common four-quadrant operation of SRM is the application in electric vehicles and rail transportation. In such condition, the SRM load can be considered constant and higher level controller or human manipulation can help realize control strategies switching for forwarding, braking and reversing [15]. Reference [16] proposed an automatic switching method of four-quadrant speed control method for electrical vehicles based on machine conditions including mover speed, position, phase inductance and inductance slope.

In summary, many researches have proposed effective control methods to address the principal drawbacks of switched reluctance machines. Most of existing studies aim at speed control applications mainly focused on electric vehicles, while the working condition of WEC is different. One major difference is that LSRM in WEC is oscillating at force mode without a speed closed loop. Most of existing FSF-based force ripple suppression methods are basically designed for switched reluctance machines working at a constant speed and load with a speed closed loop, which means these methods cannot directly apply to WEC. The dynamics of LSRM in WEC is an oscillating system with varying external wave forces, that is to say, the four- quadrant operation of the LSRM in a WEC is naturally determined and switched by its dynamic behaviors unlike in electric vehicle application that the operation quadrant is determined by higher level controllers or human manipulation. These factors cause that existing control methods are not applicable in wave energy application.

Therefore, this paper proposes a four-quadrant force control with minimal ripple for LSRM working at force mode without a speed closed loop in wave energy application. The force ripple is suppressed using FSF considering copper loss and reactive power. The four-quadrant operation is based on only current information without the knowledge of inductance slope, speed closed loop or higher controller assistance. Simulation results validate the proposed method and indicate that LSRM can be applied in direct drive WEC. The rest of this paper is organized as follows: The proposed FSF is analyzed in Sec. II. Sec III presents the four-quadrant control method. Sec IV discusses the current controller design and the simulation results are illustrated in Sec. V. Sec. VI concludes the paper.

II. FSF Considering Copper Loss and Reactive Power

The studied machine in this paper is a novel 6-4 linear tubular switched reluctance machine. The 3D diagram and its cross-section are illustrated in Fig.1.

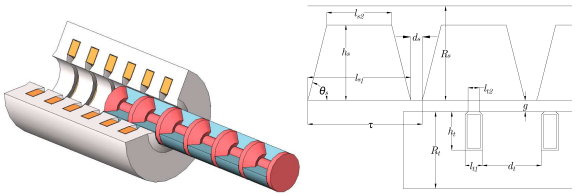

Fig.1. Dimensions of the studied 6-4 linear tubular SRM.

The detail dimensions of this machine are given in Table I.

TABLE I
Specific dimensions of the studied machine

parameters	meanings	values (mm)
τ	pole pitch	36.163
R_s	stator radius	21.378
R_t	mover radius	48.022
g	air gap	0.6
d_s	stator slot spacing	2.813
h_s	stator slot height	15.269
l_{s1}	stator slot length1	33.350
l_{s2}	stator slot length2	10.849
d_t	mover slot spacing	15.296
h_t	mover slot height	32.753
l_{t1}	mover slot length1	8.813
l_{t2}	mover slot length2	2.813

The 6-4 LRSM can be modelled as three inductors that varies with respect to mover position. According to the inductance slope, three phases conduct current alternatively to form unidirectional motion. The typical drive circuit is the asymmetric bridge circuit as shown in Fig. 2.

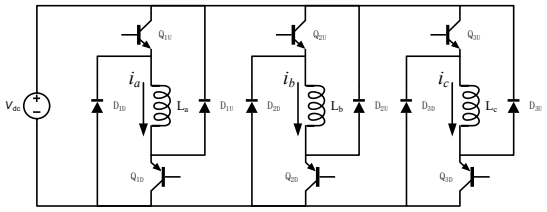

Fig. 2. Drive circuit for a 6-4 LSRM

The voltage and force equations of LSRM are as follows:

$$u_{ph} = i_{ph}R_{ph} + L_{ph}(z)\frac{di_{ph}}{dt} + \frac{dL_{ph}(z)}{dz}i_{ph}\dot{z}$$
$$F = \sum F_{ph} = \sum \frac{1}{2}i_{ph}^2\frac{dL_{ph}(z)}{dz} \quad (1)$$

where $u_{ph}, i_{ph}, R_{ph}, \lambda_{ph}, L_{ph}$ and z denote the phase voltage, current, resistance, flux, inductance and mover position, respectively. And Fig. 3 shows the inductance curves of the LSRM studied in this paper, the LSRM design is based on [7] and the data is calculated through finite element software.

During commutation, the total force is the sum of forces generated by the two conducted phases. FSF method apportions the currents of each phase to make the total force smooth:

$$\frac{1}{2}\frac{dL_1}{dz}i_1^2 + \frac{1}{2}\frac{dL_2}{dz}i_2^2 = F_r \quad (2)$$

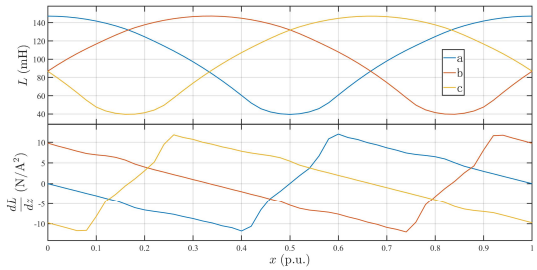

Fig. 3. Inductance characteristics of the studied LSRM

where F_r denotes the force reference, and subscripts 1 and 2 denote the outgoing phase and incoming phase, respectively. It is evident that there are infinite combinations of i_1 and i_2 which satisfy (2). Therefore, more constraints are required to solve this problem. It is common to minimize the copper loss during commutation, which is:

$$\min: i_1^2 + i_2^2 \tag{3}$$

Let

$$M_1(z) = \frac{dL_1}{dz}, M_2(z) = \frac{dL_2}{dz} \tag{4}$$

The theoretical solution to (2) and (3) can be derived:

$$\begin{cases} i_1 = \sqrt{\dfrac{2F_r}{M_1}}, M_1 \geq M_2; \\ i_2 = 0 \end{cases} \begin{cases} i_1 = 0 \\ i_2 = \sqrt{\dfrac{2F_r}{M_2}}, M_1 < M_2 \end{cases} \tag{5}$$

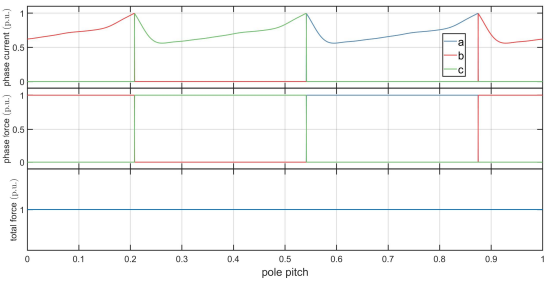

Fig.4. Theoretical FSF results considering only copper loss.

Fig.4 illustrates waveforms of the phase current, phase force and total force. It can be observed that the phase current and force profiles are all step functions. While the current rate of change is subject to the DC bus voltage in practice, a step current profile cannot be realized. Therefore, the FSF problem requires another constraint.

Taking a further analysis of the commutation process, the current of outgoing phase flows back to DC bus and decreases, while the incoming phase absorbs energy from DC bus and the current increases, this process can be illustrated by Fig. 5.

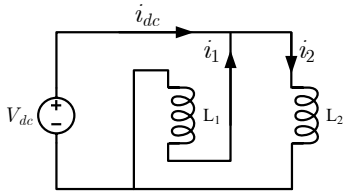

Fig. 5. Current status during commutation process

The current of DC bus is the difference between i_1 and i_2. In the beginning of commutation, $i_1 > i_2$, the DC bus current is negative, by the end of commutation, $i_1 < i_2$, the DC bus current turns positive. This indicates that part of energy of phase 1 flows back to DC bus first and then flows to phase 2, which results in reactive power during commutation. Too much reactive power increases the capacity requirement of DC bus. Hence, we can optimize the copper loss and reactive power using FSF. The reactive power is hard to quantify but we can infer that the magnitude of difference between i_1 and i_2 is proportional to the magnitude of reactive power. Therefore, we can propose the optimized objective function:

$$\min: f(x) = \frac{1}{2}\left[\alpha\left(i_1^2 + i_2^2\right) + (1-\alpha)\left(i_1 - i_2\right)^2\right] \tag{6}$$

α is the weight coefficient between copper loss and reactive power. In addition, the current rate of change cannot exceed the driving capability of DC bus:

$$\begin{aligned} \frac{di_{ph}}{dt} &\leq \frac{1}{L_{ph}}\left(V_{dc} - R_{ph}i_{ph} - \frac{dL_{ph}(z)}{dz}i_{ph}\dot{z}\right) \\ \frac{di_{ph}}{dt} &\geq \frac{1}{L_{ph}}\left(-V_{dc} - R_{ph}i_{ph} - \frac{dL_{ph}(z)}{dz}i_{ph}\dot{z}\right) \end{aligned} \tag{7}$$

In summary, the proposed FSF is an optimization problem to minimize (6) subject to (2) and (7).

The analytic solution can be derived based on KKT qualification. The analytic solution without considering (7) is as follows:

$$\begin{aligned} i_1 &= \sqrt{\frac{2F_r}{M_1}}\cos\beta \\ i_2 &= \sqrt{\frac{2F_r}{M_1}}\sin\beta \\ \beta &= \frac{1}{2}\operatorname{atan}\frac{2\sqrt{M_1M_2}(1-\alpha)}{M_1 - M_2} + \frac{k}{2}\pi \end{aligned} \tag{8}$$

where k is arbitrary integer to make $\beta \in [0, \pi/2]$. If (8) does not satisfy (7), test all boundary points to make (i_1, i_2) satisfy (2) and choose the boundary point that minimizes (6) as the FSF solution. Fig.6 shows the FSF results considering copper loss, reactive power and current driven capability of DC bus.

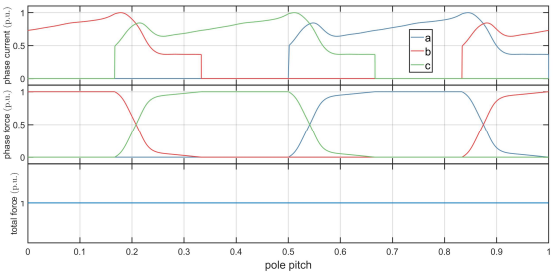

Fig.6. Theoretical FSF results considering copper loss and reactive power

III. Four-Quadrant Operation in Force Mode

It can be observed that FSF calculates the current references according to the force reference and inductance which is a function of mover position. The FSF has nothing to do with the operation mode of LSRM and is similar to LPMSM force control. In LPMSM control, the currents can be controlled through PI regulators based on SVPWM algorithm, and the motor will operate in all quadrants naturally. However, the models between LPMSM and LSRM are quite different, which

means SVPWM is not suitable for SRM current control. Therefore, to smooth the force and realize four-quadrant operation in force mode, the only thing to do is to control the currents of motor to follow the current references derived from FSF fast and accurately.

To control the current, the tracking error defined by the difference between current reference and actual current is prerequisite, if the error is negative, the switching state that increases the current should be selected, while the switching state that decreases the current should be selected once the tracking error is positive. And PWM is adopted to improve the current tracking performance by adjusting the duty ratio. The duty ratio is usually calculated by a PI regulator:

$$d = k_p e + k_i \int e dt \tag{9}$$

Where k_p and k_i are the proportional and integral coefficients of the PI regulator, e is the tracking error and d is the duty ratio.

According to the topology of the drive circuit as shown in Fig. 2, using(s_u, s_d) to denote the switch state of up switch and down switch of one phase, where 1 means on and 0 means off. There are four combinations of s_u and s_d while two have identical effect. Then we have three different switch states that apply different voltages to LSRM: $+V_{dc}$ under (1, 1) denoted by +1,$0V_{dc}$ under (1, 0) or (0, 1) denoted by 0 and $-V_{dc}$ under (0, 0) denoted by -1, as shown in Fig. 7.

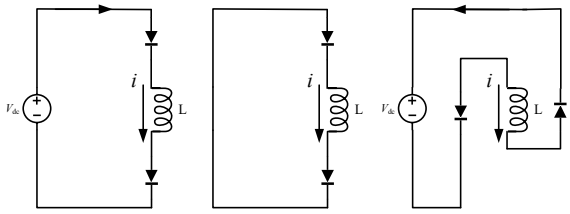

Fig. 7. Equivalent circuits under different switch states

It is obvious that the phase current increases under +1 while decreases under -1, which means the power flow into or out of the machine, respectively. However, the current trend under 0 is indeterminate and depends on whether LSRM is operating as a motor or generator.

The current control can be realized by switching from +1 to -1, namely hard chopping mode. However, hard chopping mode will drastically increase the DC bus current fluctuation and phase current ripple. Another way to realize current control uses all three switch states and avoids switching from +1 to -1, namely soft chopping mode [17].

In soft chopping mode, the current control strategies in different operation quadrants are different due to the uncertainty of switch state 0. And Fig. 8 illustrates the different current control strategies.

No matter which quadrant the LSRM is operating in, there are three control stages. The first is the excitation stage (Ext). In this stage, positive voltage is applied to excite the phase winding to generate sufficient magnetic field cause that there are no magnets in the LSRM. The second is the motor mode or generator mode. In motor mode, positive voltage is applied to convert electrical energy into mechanical energy, while in generator mode, negative voltage is applied to convert

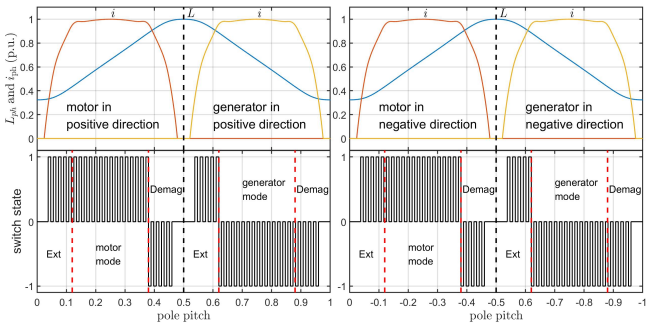

Fig. 8. Current control strategies under different operation quadrants.

mechanical energy into electrical energy. The third is demagnetization stage (Demag), negative voltage is applied to release the energy of magnetic field and make it return to DC bus. Therefore, the problem of four-quadrant operation is to determine the shift timing among excitation, motor operation, generator operation and demagnetization stages. However, this is still hard to realize cause the shift timing is related to mover position, operation mode and many other factors.

From the perspective of switch states, we can find that the current control strategy in excitation and motor operation stage is the same, which is PWM control using switch states +1 and 0, the duty ratio can be defined as the proportion of switch state +1 in a PWM cycle. This PWM control is denoted by +1 mode. In a similar way, -1 mode is the PWM control using switch states 0 and -1 in demagnetization and generator operation. The duty ratio is the proportion of switch state 0 in a PWM cycle. Based on such analysis, no matter which quadrant the LSRM is operating in, the current control first uses +1 mode PWM control and then shifts to -1 mode PWM control. The slight difference is the mode shift timing and the point is how to determine the shift timing.

Considering the dynamic process of the current response under different PWM mode, Fig. 9 illustrates the possible scenarios.

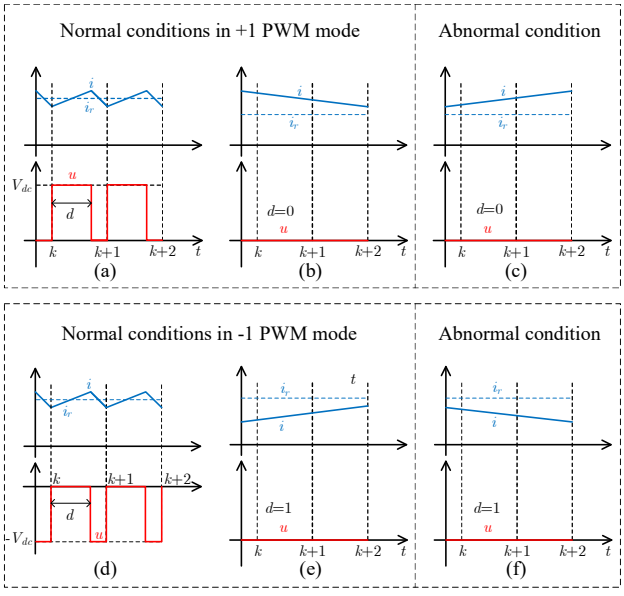

Fig. 9. Analysis of dynamic process of current response

Fig. 9(a) illustrates the steady-state current response under +1 PWM mode, in one PWM cycle with duty ratio *d,* the actual

current i increases first and decreases then, the average is consistent with the reference i_r. In an extreme case, i_r is less than i for several PWM cycles, this will lead d to 0, which means that the switch state keeps at 0 in one PWM cycle so that the actual current decreases fast to track the reference. Though i is not following i_r in such case, the absolute tracking error should decrease when $d = 0$, as illustrated in Fig. 6(b). However as mentioned before, the current variation trend is indeterminate under 0 switch state. Another extreme case which is abnormal in +1 PWM mode is illustrated in Fig. 6(c), i and the absolute tracking error both increase when $d = 0$. This means that the PWM mode should change to -1 mode and select switch state -1 to decrease the current to follow the reference. Therefore, we can determine the shift timing from +1 PWM mode to -1 PWM mode only using current information.

Similar analysis can be conducted to determine the shift timing from -1 PWM mode to +1 PWM mode. Fig. 9(d) illustrates the steady-state current response under -1 PWM mode. In an extreme case, i_r is larger than i for several PWM cycles, this will lead d to 1, which means that the switch state keeps at 0 in one PWM cycle so that the actual current increases fast to track the reference. The absolute tracking error should decrease when $d = 1$, as illustrated in Fig. 6(e). However, if i decreases and the absolute tracking error increases when $d = 1$ as illustrated in Fig. 9(f), this means that the PWM mode should be switched to +1 mode.

Therefore, the shift timing for LSRM current control PWM mode selection is obtained. Note that this method requires only the current information and it is independent of the specific LSRM model parameters and no need of speed information of speed closed loop, which indicates it is an easy-to-implement method. Fig. 10 illustrates the flowchart of proposed method. Since noise in current measurement may cause misjudgment, a counter to record the numbers of abnormal cases is adopted, and the PWM mode should be switched once the count exceeds the threshold.

IV. Current Controller Design

Referring to current control of LPMSM, the transfer function diagram of LSRM current control is illustrated in Fig. 11. The drive circuit can be equivalent as a first order system with time constant that equals to PWM period T_s, and the LSRM can be modeled as a resistance-inductance system, and the emf u_d can be regarded as the disturbance input.

Proper PI parameters can achieve good current control performance. However, inductance of LSRM varies with respect to the mover position and the maximum is almost 4 times the minimum. If PI parameters are constant, the performance will degrade due to the inductance variation.

According to the optimal design for LPMSM current control, the parameters of the PI regulator should be:

$$k_p = \frac{0.5L_{ph}}{V_{dc}T_s} \qquad k_i = \frac{R_{ph}}{V_{dc}T_s} \tag{10}$$

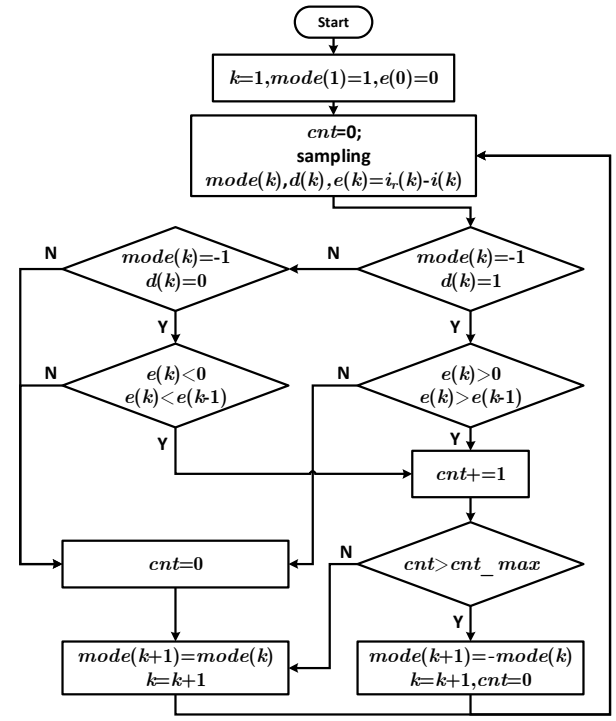

Fig. 10. Flowchart of four-quadrant operation control.

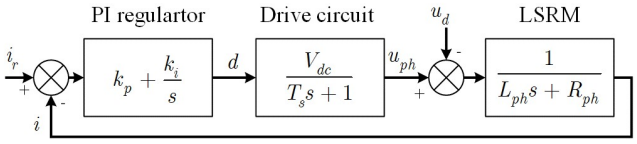

Fig. 11. Transfer function diagram of LSRM current control

In such settings the performance of current response will be optimal. Therefore, we can automatically adjust the parameters by substituting the inductance of current position into (10). And Fig. 12 illustrates the overall schematic diagram of force control for LSRM as the linear generator in WEC.

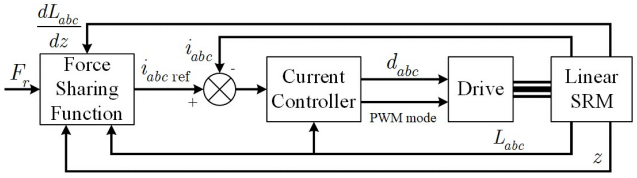

Fig. 12. Force control for LSRM as the linear generator in WEC

The FSF unit calculates the current references of each phase based on force reference and motor state information including motor velocity, inductance and inductance slope with respect to mover position. Based on the current tracking errors, the current controller determines the duty ratio and PWM mode to control the asymmetric bridge circuit to drive the motor.

V. Simulation Results and Discussions

A LSRM simulation model is established in MATLAB/Simulink platform to validate proposed algorithm

A. Performance comparison between proposed FSF and existing methods.

Performance indexes of different FSF methods including proposed FSF, linear FSF, cubit FSF, sinusoid FSF and

exponential FSF were discussed. Based on (6), the performance index can be decomposed into two parts: copper loss part J_1 and reactive power part J_2 .The overall performance is the sum of J_1 and J_2 with a weight coefficient α:

$$J_1 = \frac{1}{2}\left(i_1^2 + i_2^2\right)$$
$$J_2 = \frac{1}{2}\left(i_1 - i_2\right)^2 \tag{11}$$
$$J = \alpha J_1 + \left(1-\alpha\right) J_2$$

J, J_1 and J_2 of different FSF methods under different weight coefficients are listed in Table II,Table III and Table IV, respectively.

TABLE II
Performance comparison of J between different FSF methods

α	proposed	linear	cubic	sinusoidal	exponential
0	0.019	0.215	0.328	0.340	0.328
0.2	0.430	0.627	0.685	0.692	0.624
0.4	0.817	1.040	1.041	1.044	0.920
0.5	1.000	1.246	1.220	1.220	1.068
0.6	1.173	1.452	1.398	1.396	1.216
0.8	1.484	1.865	1.755	1.748	1.508
1	1.742	2.277	2.111	2.100	1.785

TABLE III
Performance comparison of J_1 between different FSF methods

α	proposed	linear	cubic	sinusoidal	exponential
0	1.122	1.204	1.116	1.110	0.956
0.2	1.074	1.204	1.116	1.110	0.956
0.4	1.024	1.204	1.116	1.110	0.956
0.5	1.000	1.204	1.116	1.110	0.956
0.6	0.976	1.204	1.116	1.110	0.956
0.8	0.934	1.204	1.116	1.110	0.944
1	0.921	1.204	1.116	1.110	0.944

TABLE IV
Performance comparison of J_2 between different FSF methods

α	proposed	linear	cubic	sinusoidal	exponential
0	0.177	1.977	3.023	3.136	3.022
0.2	0.274	1.977	3.023	3.136	3.022
0.4	0.650	1.977	3.023	3.136	3.022
0.5	1.000	1.977	3.023	3.136	3.022
0.6	1.511	1.977	3.023	3.136	3.022
0.8	3.301	1.977	3.023	3.136	3.653
1	6.838	20.986	19.455	3.136	3.653

The solution of the proposed method has been analyzed in the previous section. For the FSF methods based on specific functions, the optimized parameters are the turn-on and turn-off position. In this work, these two parameters are derived based on method of exhaustion. For better comparison, the data are normalized based on the values of J, J_1 and J_2 under α=0.5.

It is obvious that the proposed method exhibits best performance. Along with α change, there are distinct changes in the performance of the proposed FSF. The increase of α means that the copper loss plays a more import part and thus J_1 decreases. Otherwise J_2 decreases once α decreases. However, the performance indexes of FSF methods based on specific functions hardly change. This illustrates there is little room for adjustment of these methods. Besides, these methods are related to conventional control method of LSRM, the optimal turn-on and turn-off position are hard to determine under changing operation conditions and are not able to realize four-quadrant operation.

B. Current control Results

Fig.13 illustrates the control results using conventional LSRM control method, which is the fixed turn-on and turn-off position control. The current reference is set to 2A. The result manifests there exists drastic force ripple during commutation region. Besides, in single-phase conduction region, the ripple is still obvious due to the mismatch between linear current and nonlinear inductance characteristics. Such force response performance is not suitable to use LSRM as a generator for WEC.

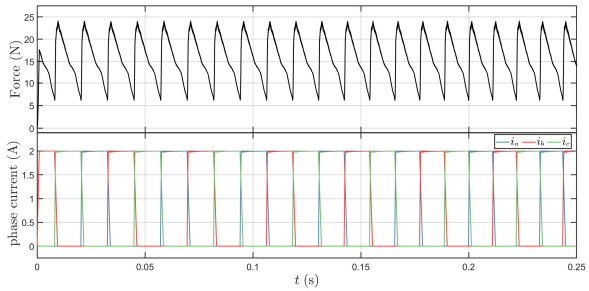

Fig.13. Force control results using conventional method.

Fig.14 shows the force control results using proposed FSF method with constant PI parameters. The force reference is 20N.

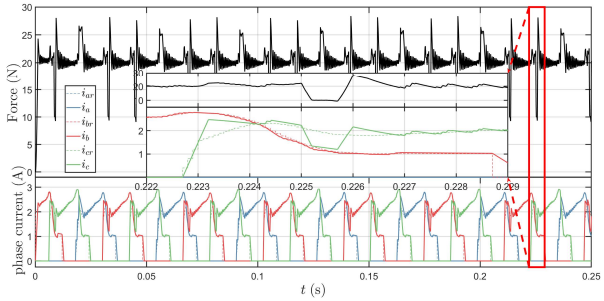

Fig.14. Force control results using proposed FSF method (constant PI parameters)

It can be observed that the force ripple has been significantly suppressed compared with the conventional method. However, force rises and falls during commutation. From the enlarged image of one commutation region in Fig.14, it can be clearly seen that the actual current fails to follow the reference within some intervals. The simulation results coincide with the theoretical analysis that the constant parameter PI regulator may incur performance degradation due to the varying inductance with a broad range. As a result, the force fluctuates. This can be solved using variable parameters PI controller, Fig. 15 shows the results.

After using variable parameters PI controller, the current response performance is guaranteed in each position. However, the force response curve is not an ideal line with amplitude that equals to the force reference. Through observation of the current curve in the enlarge zone of Fig. 15, the actual current has slight ripple, which is inevitable in PWM current control. And this slight ripple results in slight fluctuation in motor force. In addition, the inherent and inevitable delay of a digital cont-

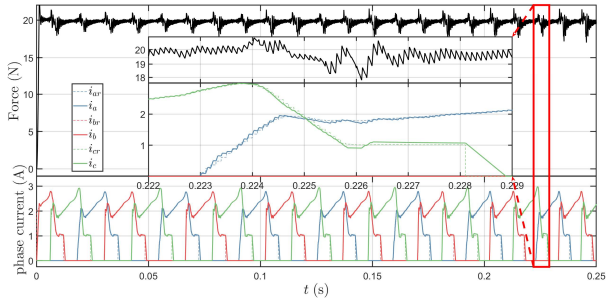

Fig. 15. Force control results using proposed FSF method (variable PI parameters, 10kHz PWM frequency)

rol system will also make the actual current unable to ideally track the current reference. This delay will also have a negative effect of smoothing the output force of LSRM. The PWM frequency can be increased to counter the force ripple caused by current ripple and digital delay. Fig. 16 illustrates the results with 20kHz PWM frequency.

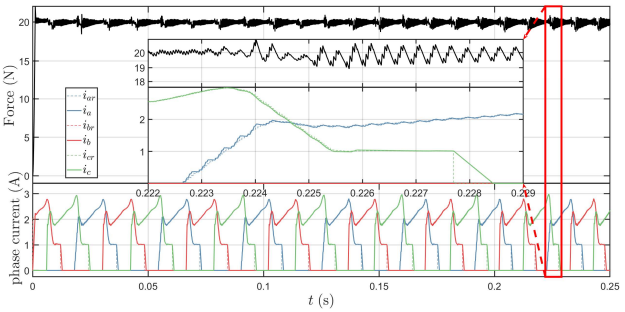

Fig. 16. Force control results using proposed FSF method (variable PI parameters, 20kHz PWM frequency)

It can be seen that the force ripple under 20kHz is smaller than that under 10kHz. It is reasonable to infer that the force ripple can be suppressed further if increasing the PWM frequency further. However, 20kHz is the limit for an IGBT-based circuit and this force ripple is small enough and tolerable for a generator in WEC.

C. *Four-quadrant operation control Results*

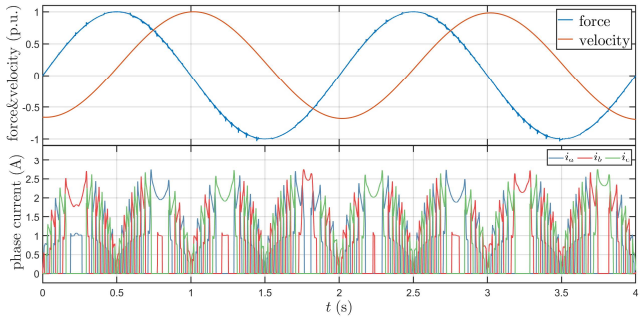

Fig. 17. Four-quadrant force control results.

Fig. 17 illustrates the force control results of LSRM driven by sinusoidal external force. The force reference is also sinusoidal with a phase offset. In such case, the motor should be operating in four quadrants in theory. The results coincide to the theoretical analysis and show that the motor force is smooth and the operation directions and modes of the LSRM are changing, which means the proposed four-quadrant control method is effective.

VI. Conclusion

The nonlinearity of LSRM makes it unable to act as the WEC generator if conventional LSRM control methods are adopted. Therefore, this paper proposed a control method for LSRMs using as the generator in direct drive WEC.

Considering the control requirements of WEC, the LSRM should operate in four-quadrant force mode with accurate force control. FSF considering copper loss and reactive power is adopted to suppress force ripple and an easy-to-implement LSRM four-quadrant control method is put forward only using current information. Simulation results indicate that the force ripple can be effectively suppressed and the LSRM can operate in four-quadrant force mode smoothly, which means the LSRM is a promising alternative generator for direct drive WEC. Compared with some existing methods, the proposed FSF method can optimize not only the copper loss under current and voltage constraints but also the reactive power during commutation to increase the power factor. In addition, the proposed four-quadrant control method is applicable in wave energy application, which is the four-quadrant operation in force mode with no speed closed loop and varying external forces. This method can be implemented only using current feedback information other than existing methods that require higher controller assistance or human manipulation.

The proposed control method is not only applicable to LSRM used in direct drive WEC, but also other four-quadrant force control applications and high-performance speed control incorporated with speed loop. Besides, this control method can be easily modified to control rotational switched reluctance machines.

REFERENCE

[1] X. Xiao, X. Huang, and Q. Kang, "A hill-climbing-method-based maximum-power-point-tracking strategy for direct-drive wave energy converters," *IEEE Trans. Ind. Electron.*, vol. 63, no. 1, pp. 257-267, 2015.

[2] J. Ji, J. Zhao, W. Zhao, Z. Fang, G. Liu, and Y. Du, "New High Force Density Tubular Permanent-Magnet Motor," *IEEE Transactions on Applied Superconductivity,* vol. 24, no. 3, pp. 1-5, 2014, doi: 10.1109/TASC.2013.2284481.

[3] Y. Zou, K.-W. E. Cheng, N. C. Cheung, and J. Pan, "Deformation and noise mitigation for the linear switched reluctance motor with skewed teeth structure," *IEEE Transactions on Magnetics,* vol. 50, no. 11, pp. 1-4, 2014.

[4] D. Wang, C. Shao, and X. Wang, "Performance analysis and design optimization of an annular winding bilateral linear switch reluctance machine for low cost linear applications," *IEEE Transactions on Applied Superconductivity,* vol. 26, no. 7, pp. 1-5, 2016.

[5] D. Wang, X. Wang, and C. Zhang, "Performance analysis of a high power density tubular linear switch reluctance generator for direct drive marine wave energy conversion," in *2014 17th International Conference on Electrical Machines and Systems (ICEMS)*, 2014: IEEE, pp. 1781-1785.

[6] R. Mendes, M. Calado, S. Mariano, and C. Cabrita, "Design of a tubular switched reluctance linear generator for wave energy conversion based on ocean wave parameters," in *International Aegean Conference on Electrical Machines and Power Electronics and Electromotion, Joint Conference*, 2011: IEEE, pp. 146-151.

[7] D. Wang, C. Shao, X. Wang, and C. Zhang, "Performance characteristics and preliminary analysis of low cost tubular linear switch reluctance generator for direct drive WEC," *IEEE Transactions on Applied Superconductivity,* vol. 26, no. 7, pp. 1-5, 2016.

[8] S. K. Sahoo, S. Dasgupta, S. K. Panda, and J.-X. Xu, "A Lyapunov

function-based robust direct torque controller for a switched reluctance motor drive system," *IEEE Transactions on Power Electronics,* vol. 27, no. 2, pp. 555-564, 2011.

[9] X. Xue, K. Cheng, and S. Ho, "Optimization and evaluation of torque-sharing functions for torque ripple minimization in switched reluctance motor drives," *IEEE transactions on power electronics,* vol. 24, no. 9, pp. 2076-2090, 2009.

[10] V. P. Vujičić, "Minimization of torque ripple and copper losses in switched reluctance drive," *IEEE transactions on power electronics,* vol. 27, no. 1, pp. 388-399, 2012.

[11] J. Ye, B. Bilgin, and A. Emadi, "An offline torque sharing function for torque ripple reduction in switched reluctance motor drives," *IEEE Transactions on energy conversion,* vol. 30, no. 2, pp. 726-735, 2015.

[12] Q. Sun, J. Wu, C. Gan, and J. Wang, "A novel boost chopper converter-based torque sharing function control strategy for switched reluctance motors," in *2017 20th International Conference on Electrical Machines and Systems (ICEMS)*, 2017: IEEE, pp. 1-6.

[13] M. J. Kermanipour and B. Ganji, "Modification in geometric structure of double-sided axial flux switched reluctance motor for mitigating torque ripple," *Canadian Journal of Electrical and Computer Engineering,* vol. 38, no. 4, pp. 318-322, 2015.

[14] S. KUAI, P. WANG, and J. CHENG, "Four-quadrant position sensorless technology of switched reluctance motors based on variable coefficients inductance mode," *Transactions of China Electrotechnical Society,* vol. 29, no. 7, pp. 114-125, 2014.

[15] A. Y. Yang, B. Y. Zhang, and C. S. Wang, "Four-quadrant control of dsp-based switched reluctance drives for EV," in *2007 2nd IEEE Conference on Industrial Electronics and Applications*, 2007: IEEE, pp. 2162-2167.

[16] I. Kioskeridis and C. Mademlis, "A unified approach for four-quadrant optimal controlled switched reluctance machine drives with smooth transition between control operations," *IEEE transactions on power electronics,* vol. 24, no. 1, pp. 301-306, 2008.

[17] M. Blanco, G. Navarro, and M. Lafoz, "Control of power electronics driving a switched reluctance linear generator in wave energy applications," in *2009 13th European Conference on Power Electronics and Applications*, 8-10 Sept. 2009 2009, pp. 1-9.

Xuanrui Huang (S'17–M'20) was born in Xinjiang Province, China, in 1991. He received the B.E. degree in 2013 from Tsinghua University, Beijing, China, where he is currently working toward the Ph.D. degree in the Department of Electrical Engineering.

His research focuses on permanent-magnet synchronous motor control, wave energy and switched reluctance machines.

Zechuan Lin was born in Fujian Province, China, in 1996. He received the B.E. degree from North China Electric Power University, Beijing, China, in 2019. He is currently working toward the Ph.D. degree in Tsinghua University, Beijing, China.

His research focuses on wave energy conversion and switched reluctance machines.

Xi Xiao (M'07) was born in Hunan Province, China, in 1973. He received the B.E., M.E., and Ph.D. degrees from Saint Petersburg State Technical University, Saint Petersburg, Russia, in 1995, 1997, and 2000, respectively.

Since 2001, he has been with the Department of Electrical Engineering, Tsinghua University, Beijing, China, where he is currently a Full Professor and the Vice Dean of the department. His main areas of research interest are permanent magnet synchronous motor control, power electronics, and renewable energy.